Simulation of Taylor Flow in Capillaries Based on the Volume-of-Fluid Technique

M. K. Akbar*,† and S. M. Ghiaasiaan*,‡

G. W. Woodruff School of Mechanical Engineering, Georgia Institute of Technology Savannah, Savannah, Georgia 31407, and G. W. Woodruff School of Mechanical Engineering, Georgia Institute of Technology, Atlanta, Georgia 30332-0405

Taylor flow, a flow regime characterized by Taylor bubbles separated by liquid slugs that do not contain entrained micro bubbles, is a predominant gas−liquid two-phase flow regime in capillaries and minichannels (channels with hydraulic diameters in the 0.1−1 mm range), and it occurs in monolithic catalytic converters and other multiphase reactors. Taylor flow regime is morphologically relatively simple and has been modeled in the past using computational fluid dynamics (CFD) methods. However, most of the past CFD models have either assumed a fixed gas−liquid interfacial geometry or have modeled the gas−liquid interphase movement based on the method of spines, which imposes some restrictions on the free movement of the interface. In this study, we examine the feasibility of CFD modeling of the Taylor flow regime in capillaries by using the volume-of-fluid (VOF) technique for the motion of the gas−liquid interphase. It is shown that such a model predicts well the experimental data and empirical correlations relevant to the hydrodynamics of capillaries. Improved correlations for slug length and pressure drop in capillaries are also suggested based on available experimental data.

1. Introduction

The Taylor bubble (bubble train) regime is an important two-phase flow pattern in capillaries and minichannels that covers an extensive portion of their two-phase flow regime maps.[1,2] Current interest in Taylor bubble flow in capillaries is primarily due to their application in monolithic catalyst converters and other multiphase reactors. Monolithic converters made of arrays of parallel small channels with diameters of ∼1 mm provide high catalytic surface concentrations, highly efficient mass transfer, and low pressure drop. Heiszwolf et al.[3] have shown that the performance of a loop based on a cocurrent downflow monolith can be superior to the performance of a stirred-tank reactor. Nijhuis et al.[4] demonstrated experimentally the advantages of a pilot three-phase catalyst monolith over an equivalent trickle-bed reactor.

Most of the published research is focused on the hydrodynamic and transport processes in a single capillary, however. Two-phase flow through an array of parallel channels can lead to undesirable flow instability and oscillations. Accurate and reliable models for the behavior of Taylor flow is, thus, needed in order to develop strategies for avoiding these and other undesirable phenomena. The pressure drop, the slug length, and the absolute velocity of Taylor bubbles are among the important hydrodynamic parameters that need to be predicted.

Bretherton[5] investigated the advancement of gas into a liquid-filled channel and showed that the thickness of the liquid film deposited on the wall depended on the capillary number *Ca*, and for the limit of $Ca \rightarrow 0$, $2\delta/D = 1.34Ca^{2/3}$. For finite *Ca* values, the latter expression is valid if D is replaced with $D - 2\delta$. An empirical curve fit to the data of Taylor[6] obtained with different viscous oils resulted in[7]

$$\frac{2\delta}{D} = \frac{1.34Ca^{(2/3)}}{1 + 2.5 \times 1.34Ca^{(2/3)}} \tag{1}$$

The above discussion applies when inertial effects are negligible. At high values of *Ca*, inertia significantly influences the flow field and pressure distribution near the bubble tip and slightly modifies the behavior of the liquid film.[8]

In recent years, several investigators have experimentally studied the Taylor bubble regime in capillaries. Thulasidas et al.[9] performed experiments with circular and rectangular capillaries, using liquids that covered the range $Ca = 10^{-3}$−1.34. The liquid film thickness, the bubble absolute velocity, the ratio between bubble and slug lengths, and the average void fraction all were found to depend on *Ca*. In a follow-up study, Thulasidas et al.[10] used particle image velocimetry to elucidate the details of recirculation patterns in the liquid slugs. Bercic and Pintar[11] experimentally measured and empirically correlated the liquid-side volumetric mass transfer coefficient, as well as the volumetric solid−liquid mass transfer coefficient in capillaries with $D = 1.5$, 2.5, and 3.1 mm. Laborie et al.[12] conducted experiments addressing the hydrodynamic aspects of Taylor flow in vertical glass capillaries with $D = 1$, 2, 3, and 4 mm, using eight different liquids. Among their measured and correlated parameters were the Taylor bubble velocity, the bubble and liquid slug lengths, and the drift flux model (DFM) distribution coefficient, C_0. More recently, Kreutzer et al.[13] experimentally measured pressure drops in a vertical capillary with $D = 2.3$ mm, using a technique for controlling the lengths of bubbles and slugs. They defined a two-phase friction factor according to

$$\Delta P_f = 4f\frac{L}{D}\frac{1}{2}\rho_L(1 - \beta_G)(U_{LS} + U_{GS})^2 \tag{2}$$

where $\beta_G = U_{GS}/(U_{GS} + U_{LS})$. Kreutzer et al.[13] developed the following correlation based on their experimental data, with $a = 0.17$:

* To whom correspondence should be addressed. For M. K. Akbar: Tel.: (912) 966-7831. Fax: (912) 966-7928. E-mail: makbar@gtsav.gatech.edu. For S. M. Ghiaasiaan: Tel.: (404) 894-3746. Fax: (404) 894-8496. E-mail: seyed.ghiaasiaan@me.gatech.edu.

† Georgia Institute of Technology Savannah.

‡ Georgia Institute of Technology, Atlanta.

10.1021/ie0601551 CCC: $33.50 © 2006 American Chemical Society
Published on Web 06/17/2006

$$f = \frac{16}{Re}\left[1 + a\frac{D}{L_{slug}}(Re/Ca_L)^{0.33}\right] \quad (3)$$

Kreutzer et al.[13] also performed extensive computational fluid dynamics (CFD)-based simulations, noting that *Re* affected the film thickness and the bubble shape. The simulations agreed with eq 2, provided that $a = 0.07$ was used in eq 3 when calculating *f*. This discrepancy was attributed to the possibility of suppression of the gas−liquid interface motion in the experiments by surfactant contaminants.

Recently, Liu et al.[14] have experimentally studied two-phase flow hydrodynamics using air and three different liquids in vertical capillaries of circular and square cross section with hydraulic diameters in the 0.9−3 mm range. They observed four distinct flow regimes: bubbly, slug-bubbly, Taylor, and churn. They specifically studied and proposed correlations for bubble velocity, liquid slug lengths, and pressure drop. Negative frictional pressure drops were observed at low liquid velocities, which were attributed to falling liquid films.

A nonintrusive technique for the measurement of velocity and slug length in capillaries has been recently proposed by Wolffenbuttel et al.[15]

Taylor flow is morphologically simple, making it relatively easy to simulate using CFD techniques. Such simulation, of course, needs the resolution of the gas−liquid interphase. Several authors have indeed performed CFD simulations. Among the pioneers, Edvinsson and Irandoust[16] used the finite element-based FIDAP code[17] and modeled the Taylor bubble as essentially a void. They modeled the interphase by the spine method;[18] accordingly, two different types of elements, fixed and flexible, are defined, with the latter type used at the vicinity of the interphase. The nodes of the flexible elements can move in order to accommodate the motion of the interphase, but their motion is restricted to their corresponding prespecified spine lines. Edvinsson and Irandoust[16] predicted the occurrence of undulations near the bubble tail, in qualitative agreement with experimental observations. Several other investigators subsequently simulated the Taylor bubble flow, using essentially the same approach as Edvinsson and Irandoust.[16] Giavedoni and Saita[19,20] used the spine method and addressed the geometric shape of the liquid meniscus that traits long Taylor bubbles. Using a similar method, Heil[8] investigated the effect of inertia on the behavior of the liquid film surrounding a Taylor bubble. Kreutzer et al.[13] performed experimental and numerical investigations. Their numerical simulation was based on the aforementioned FIDAP code[17] and the method of spines.

Van Baten and Krishna[21,22] have recently performed extensive CFD simulations of Taylor bubble flow in capillaries, focusing on the liquid-side mass transfer processes at the gas−liquid interphase and at the solid−liquid interphase, respectively. Similar to the aforementioned studies, they modeled the bubble essentially as a void. They also assumed a fixed gas−liquid interphase (i.e., no interphase motion) and simulated the liquid flow field using the CFX version 4.4 CFD code.[23]

The above review indicates that the previously published simulations have mostly treated a Taylor bubble as an inviscid void. Furthermore, they have either assumed fixed interfacial geometry or have modeled the gas−liquid interphase motion using the method of spines. The investigations based on the latter technique have provided valuable insight into the Taylor flow. Nevertheless, the restrictions that the method of spines imposes on the motion of the interphase, and its effect on the simulations, have not been addressed. Quite recently, Taha and Cui[24] simulated the motion of Taylor bubbles in conventional large channels using the volume-of-fluid method implemented in the commercial CFD code Fluent. They showed that the technique leads to favorable prediction of velocity and wall shear distributions.

In this paper, the Taylor bubble flows in circular capillaries are simulated, where the interphase motion is tracked using the volume-of-fluid (VOF) technique. Steady-state Taylor bubble flow is considered. The simulation results are validated using the experimental data of Laborie et al.[12] and Liu et al.[14] The predicted bubble absolute velocity, slug length, and frictional pressure drop are also compared with available relevant experimental and computational results. In addition, some improved correlations are proposed based on available experimental data of Laborie et al.[12] and Liu et al.[14]

2. Modeling Approach

The forthcoming simulations were performed using the VOF option of the Fluent CFD code package.[25] Several user-defined functions (UDFs) were developed and utilized as well, however. Each simulation started with a unit cell containing a Taylor bubble and two one-half liquid slugs on both sides of the bubble. The Taylor bubble was initially composed of a cylinder and two hemispheres at its two ends. The axisymmetric flow domain was discretized with GAMBIT mesh generation software,[26] using quadrilateral cells. Finer meshes were used around the liquid−gas interface everywhere. Figure 1 depicts a typical nodalization pattern near an end of a Taylor bubble. For simulations addressing capillaries with $D = 1$ mm, the number of computational cells varied in the range of 2.4×10^4 to 4.5×10^4, and the smallest and largest cell volumes were of the order of 10^{-13} and 10^{-11} m^3, respectively. To check grid independence, the grids were refined by doubling the number of nodes for a few representative simulations. No significant differences with respect to bubble shape evolution, absolute velocity, or any other hydrodynamic parameter of interest were noticed.

Before each simulation, a steady-state liquid-only flow field was first established for a channel segment equal in length to a unit cell. The bubble was then placed at the center of the unit cell. The initial bubble pressure was set equal to $P_\infty + 2\sigma/D$, with P_∞ representing the (atmospheric) ambient pressure, and the initial bubble velocity was set equal to zero. A user-defined function (UDF) was developed whereby periodic axial and radial velocity boundary conditions were imposed at the inlet and outlet of the unit cell. The pressure at the outlet of the unit cell was set equal to P_∞. Transient computations were then continued until steady state was obtained. A dynamic mesh was used in order to move the computational domain at approximately the same velocity as the bubble. The bubble travel distance in each time step was found by volume averaging of the travel distances of all the computational cells in the bubble. The VOF scheme of Fluent was solved by the explicit Euler scheme, and the parts of the computational domain with void fractions >0.5 were considered to belong to the bubble.

3. Results and Discussion

3.1. Bubble Velocity and Drift Flux Model Parameters. Several cases of Laborie et al.[12] $D = 1$ mm data, and a few cases of Liu et al.[14] data, were simulated for verification and exploration of the model. We have focused our investigation on this size range (the minichannel size range) because the past experimental studies have shown that gas−liquid two-phase flows behave somewhat differently in larger channels.[2] The

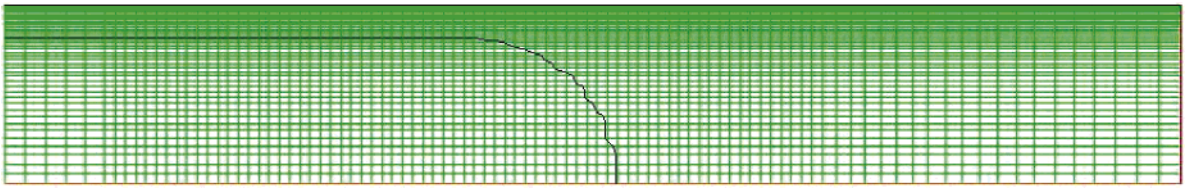

Figure 1. Nodalization scheme in the axisymmetric computational domain for a typical test case.

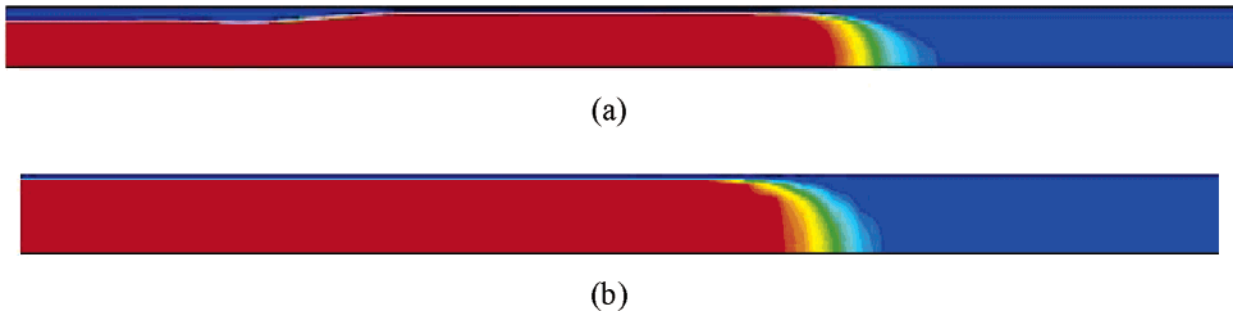

Figure 2. Typical steady-state phase distribution for bubble front (a) simulation type 1 based on Laborie et al.[12] data and (b) simulation type 2 for Liu et al.[14] data (Campaign 5).

Table 1. Fluid Properties in the Experiments of Laborie et al[12]

liquid	density (kg/m^3)	viscosity (mPa-s)	surface tension (mN/m)
fluid 2: water at 15 °C	999	1.1	73.5
fluid 3: water at 5 °C	1000	1.4	74.9
fluid 4: water/glycerol (26%)	1075	2.2	65.1
fluid 7: water/glycerol (46%)	933	1.0	32.0

simulations are divided into two groups based on the methods used for the initial estimation of the liquid film thickness surrounding the Taylor bubble. In the first group of simulations, the initial bubble radii were calculated from the experimentally estimated unit cells and bubble dimensions and gas holdup information. Gas holdup was either explicitly reported by the authors or was calculated from

$$\alpha = \frac{U_{GS}}{U_B} \tag{4}$$

This group of simulations, which start from relatively thick liquid films as their initial conditions, will be referred to as "type 1 simulations" hereafter. Another group of simulations were done by calculating the initial film thickness from eq 1. The initial film thickness in these simulations is smaller than the film thicknesses in type 1 simulations. This group of simulations will be referred to as "type 2 simulations" hereafter.

Laborie et al.[12] used glass pipes with $D = 1-4$ mm. Their data with $D = 1$ mm were used for comparison here. The experiments were done using air and seven different liquids. The properties of the fluids used in the forthcoming simulations are summarized in Table 1. Laborie et al. measured the average lengths of the Taylor bubbles and the liquid slugs for various superficial liquid and gas velocities.

Liu et al.[14] used the notation in Table 2 to identify their experiments. Their fluid properties are given in Table 3.

During a typical simulation, as the simulation proceeds, gas holdup remains approximately unchanged while the bubble and slug lengths, bubble absolute velocity, gas superficial velocity, and shapes of the bubble head and tail all change until the steady state is reached. Typical steady-state bubble front shapes for type 1 and type 2 simulations are shown in parts a and b of Figure 2, respectively.

Table 2. Experiments of Liu et al[14]

gas−liquid system	capillary hydraulic diameter (mm)	campaign
air−water circular	0.91	1
air−water circular	2	2
air−water circular	3.02	3
air−water square	2.89	4
air−ethanol circular	0.91	5
air−ethanol circular	2	6
air−ethanol circular	3.02	7
air−ethanol square	0.99	8
air−ethanol square	2.89	9
air−oil mixture circular	3.02	10
air−oil mixture square	2.89	11

Table 3. Liu et al[14] Physical Properties of Liquids Used at 298 K and 100 KPa

liquid	density (kg/m^3)	viscosity (mPa·s)	surface tension (mN/m)
water	998	0.95	72
ethanol	780	1.2	22
oil mixture	840	15.9	28

Some of the experimental data of Laborie et al.[12] are compared with type 1 simulation results in Figure 3 parts a and b, where the Taylor bubble length, L_G, is shown as a function of the bubble superficial velocity, U_{GS}. Detailed information about the experimental runs were obtained from Laborie.[27]

Except for the data representing fluid 3 with $U_{LS} = 0.49$ m/s in Figure 3a, overall, the simulation results agree well with the experimental data, in terms of both the magnitude of the predicted bubble velocities and the trends representing the effects of various properties. The simulation of other experimental data of Laborie et al., which are not shown here for brevity, showed similarly good agreement between data and predictions. For the data with $U_{LS} = 0.49$ m/s in Figure 3a, the worst simulated case predicts bubble velocity ~40% lower than the experimental data. A possible reason is that, because of the higher U_{GS}/U_{LS} and shorter liquid slug, the liquid velocity profile was significantly different than the initial parabolic profile assumed in the simulation. Thulasidas et al.[10] have observed that the flow pattern in the liquid slug is influenced by U_{GS}/U_{LS}.

For near-circular channels with $D \leq 1$ mm, the flow regimes are expected to be insensitive to the channel orientation. For some of the cases depicted in Figure 3 parts a and b, identical

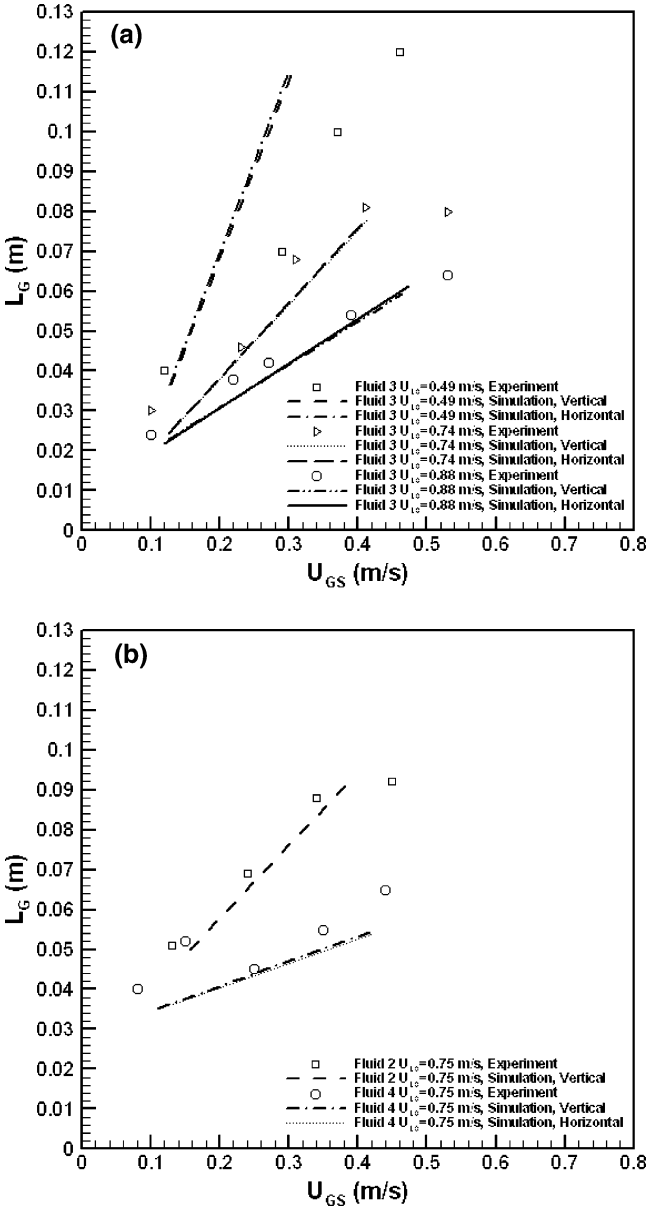

Figure 3. Comparison between the experimental data of Laborie et al.[12] and the simulations, for $D = 1$ mm, (a) Figure 11 of Laborie et al.[12] and (b) Figure 13 of Laborie et al.[12]

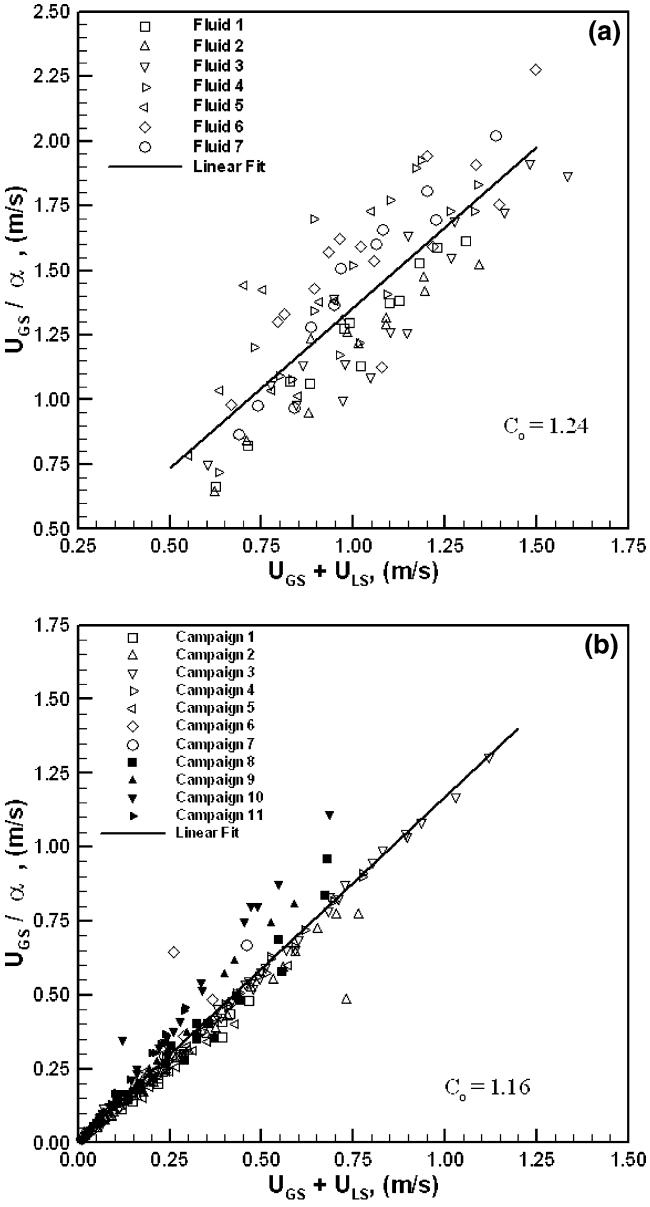

Figure 4. Predicted drift flux model (DFM) parameters based on (a) data of Laborie et al.,[12] $D = 1$ mm, (b) all data of Liu et al.[14]

type 1 simulations were repeated assuming horizontal flow configurations and compared with the vertical up-flow results. Both simulation results were quite close, as expected.

The drift flux model (DFM) has been applied to two-phase flow in capillaries and microchannels in the past. For air/water-like fluid pairs flowing in near-circular channels with $D_H \leq 1$ mm, it has been observed that the slip velocity is negligibly small in bubbly and plug/slug flow regimes.[2] Flow stratification does not occur when $D_H/\sqrt{\sigma/(g(\rho_L-\rho_G))} \leq 0.3$, furthermore,[28] and the flow regimes are insensitive to channel orientation with respect to the gravitational field. Mishima and Hibiki[29] have accordingly argued that $V_{gj} \approx 0$ for mini- and microchannels. Using their own data and the data of Kariyasaki et al.[30], Mishima and Hibiki suggested the following empirical correlation,

$$C_0 = 1.2 + 0.51\, e^{-0.692 D_H} \tag{5}$$

where D_H must be in mm. For large channels, the correlation leads to $C_0 \rightarrow 1.2$. This is in agreement with experimental observations for slug flow in conventional vertical tubes, in which $C_0 = 1.2$ when the flow in the liquid slug approaches fully turbulent conditions.[31,32] Laborie et al.,[12] in analyzing their data, noted that C_0 increased with increasing μ_L and decreased as σ increased. Accordingly, they derived a different C_0 value for each of their liquids. For their 1-mm-diameter pipe data, C_0 varied in the 1.20−1.46 range. We attempted to derive an optimum set of DFM parameters based on the experimental data of Laborie et al.[12] and Liu et al.[14] According to DFM,

$$\frac{U_{GS}}{\alpha} = C_0(U_{GS} + U_{LS}) + \frac{V_{gj}}{\alpha} \tag{6}$$

Parts a and b of Figure 4 display the data of Laborie et al. for $D = 1$ mm and all the data of Liu et al., respectively. The C_0 values for Laborie et al.[12] and Liu et al.[14] experimental data are 1.24, and 1.16, respectively. The V_{gj} values are approximately equal to zero, as expected.

For absolute bubble velocity, Liu et al.[14] proposed the following correlation,

$$\frac{U_B}{U_{GS}+U_{LS}} = \frac{1}{1-0.61Ca_L^{0.33}} \quad (7)$$

where $Ca_L = \mu_L U_{TP}/\sigma$. The data of Laborie et al.,[12] representing $D = 1$ mm, and the data of Liu et al.[14] are compared with the above correlation in Figure 5, where our simulation results are also shown for comparison. Although the correlation predicts most of the experimental data of Liu et al. well, some of the 0.91-mm-diameter circular capillary air−ethanol (Campaign 5) data are overpredicted. The correlation slightly underpredicts the $D = 1$ mm experimental data of Laborie et al. Overall, however, the agreement between the above correlation and our simulations is good.

3.2. Liquid Slug Length. Liu et al.[14] have proposed the following correlation for liquid slug length based on their own experimental data:

$$\frac{U_{TP}}{\sqrt{L_{slug}}} = 0.088 Re_G^{0.72} Re_L^{0.19} \quad (8)$$

The data of Liu et al.[14] and Laborie et al.,[12] as well as our simulation results, are plotted against this correlation in Figure 6. The correlation consistently overpredicts the data of Laborie et al. Therefore, the following correlation is proposed here, in which D, L_{slug}, and L_{UC} are in m and U_{TP} is in m/s:

$$\frac{U_{TP}^{-0.33}}{\sqrt{L_{slug}}} = 142.6\alpha^{0.56}\left(\frac{D}{L_{UC}}\right)^{0.42} Re_G^{-0.252} \quad (9)$$

The above correlation is compared with data and simulation results in Figure 7. The agreement is very good, and the correlation predicts $U_{TP}/\sqrt{L_{slug}}$ within a standard deviation of only 19.5%.

3.3. Frictional Pressure Drop. The frictional pressure gradient in a simulation dealing with vertical flow is calculated from

$$\left(-\frac{dP}{dz}\right)_f = \frac{\Delta P_f}{L_{UC}} \quad (10)$$

$$\Delta P_f = P|_{x=-(L_{UC}/2)} - P|_{x=(L_{UC}/2)} - \frac{1}{\pi(D/2)^2} g[\rho_G V_B + \rho_L(\pi(D/2)^2 L_{UC} - V_B)] \quad (11)$$

The frictional pressure gradients obtained from Liu et al.[14] experimental data for vertically upward flows are compared with several correlations in Figure 8 parts a−d. Figure 8a compares the data with the correlation of Kreutzer et al.,[13] and parts b, c, and d of Figure 8 display comparisons with the correlations of Beattie and Whalley,[33] Friedel,[34] and our forthcoming correlation (eq 12), respectively. All the correlations deviate from data at very low Re. There is considerable data scatter at the very low Re range, however, suggesting that these data should be treated with caution. The correlations of Kreutzer et al.[13] and Friedel[34] agree with the data reasonably well, when the data for $Re < 500$ are not considered. The correlation of Kreutzer et al., which agrees best with the data among the depicted correlations, underpredicts the data slightly but systematically, however.

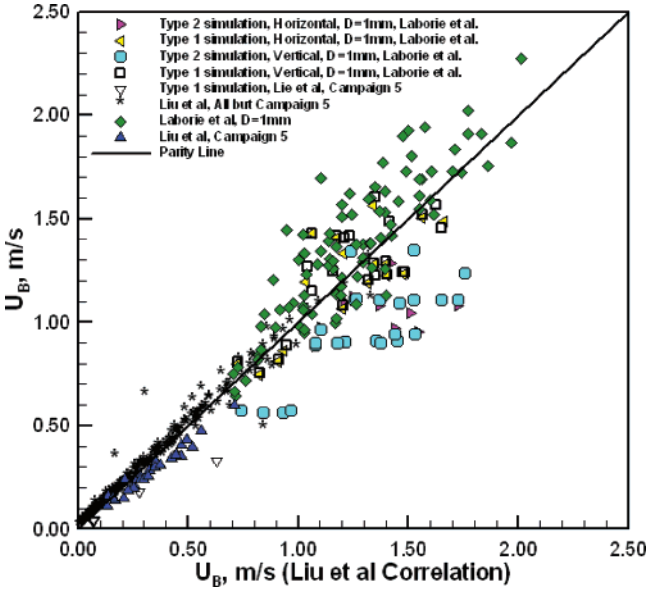

Figure 5. Comparison between the simulation results for absolute bubble velocities with the correlation of Liu et al.[14]

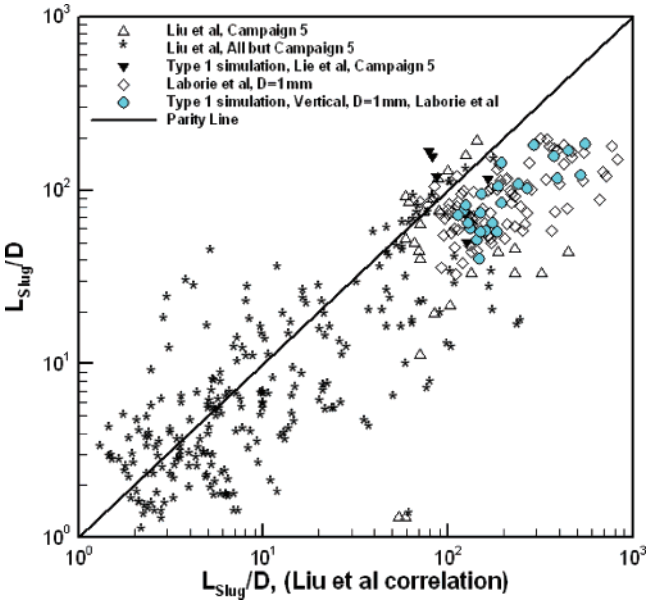

Figure 6. Comparison between the simulation results for the liquid slug length and the correlation of Liu et al.[14] (eq 8).

Better agreement can be obtained with the following correlation, as displayed in Figure 8d:

$$\left(-\frac{dP}{dz}\right)_f = 0.0012\rho_L^{2.12}\left(\frac{L_{UC}}{D}\right)^{1.06} U_{TP}^{2.16} f^{1.13}(1-\beta_G)^{1.07} \quad (12)$$

The above correlation does not systematically underpredict or overpredict the data for the $Re > 500$ range.

3.4. Liquid Film Thickness. Using the experimental data of Liu et al.[14] and Laborie et al.,[12] we estimated the liquid film thicknesses based on the information of bubble lengths, unit cell dimensions, and gas holdups assuming that bubble shapes are approximately cylindrical with hemispherical front and tail. Parts a and b of Figure 9 display the film thicknesses estimated from the experimental data and those calculated from our type 1 simulations. Since the film thickness is not uniform along an entire Taylor bubble, the film thicknesses at two locations along the bubble are shown. Figure 9a depicts the film thickness near

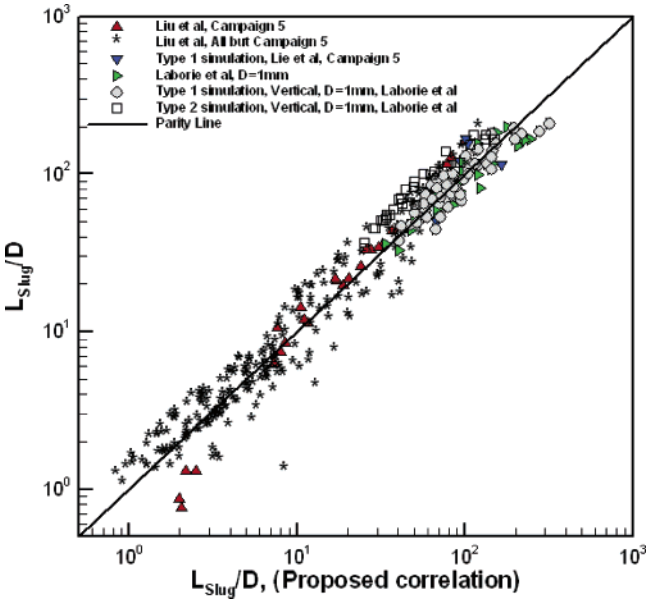

Figure 7. Comparison between the simulation results for the liquid slug length and the correlation proposed in this study (eq 9).

the center of the bubble, while Figure 9b displays the film thickness near the front end of the near-cylindrical portion of the bubble. In Figure 9a, the simulation results for the data of Liu et al. are close to the predictions of eq 1. For the experimental data of Laborie et al., although the estimated experimental film thicknesses are in good agreement with the simulations, they both disagree with eq 1 rather significantly. As noted in Figure 9b, however, the simulation results are everywhere within a factor of ~2 from the predictions of eq 1. Previously published simulations that have used the method of spines for tracking the liquid−gas interphase appear to have predicted film thicknesses close to Bretherton's theory. Aussillous and Quéré,[7] however, noted that Bretherton's theory is accurate for $Ca \rightarrow 0$ only and underpredicts the liquid film thickness because of its neglection of the effect of inertia. The underprediction of $2\delta/D$ could, in fact, reach ~50% or higher for Ca ≥ 0.03. Our simulation results, thus, display a similar trend.

4. Conclusions

Taylor flow regime (also referred to as slug flow) is a predominant gas−liquid two-phase flow regime in capillaries

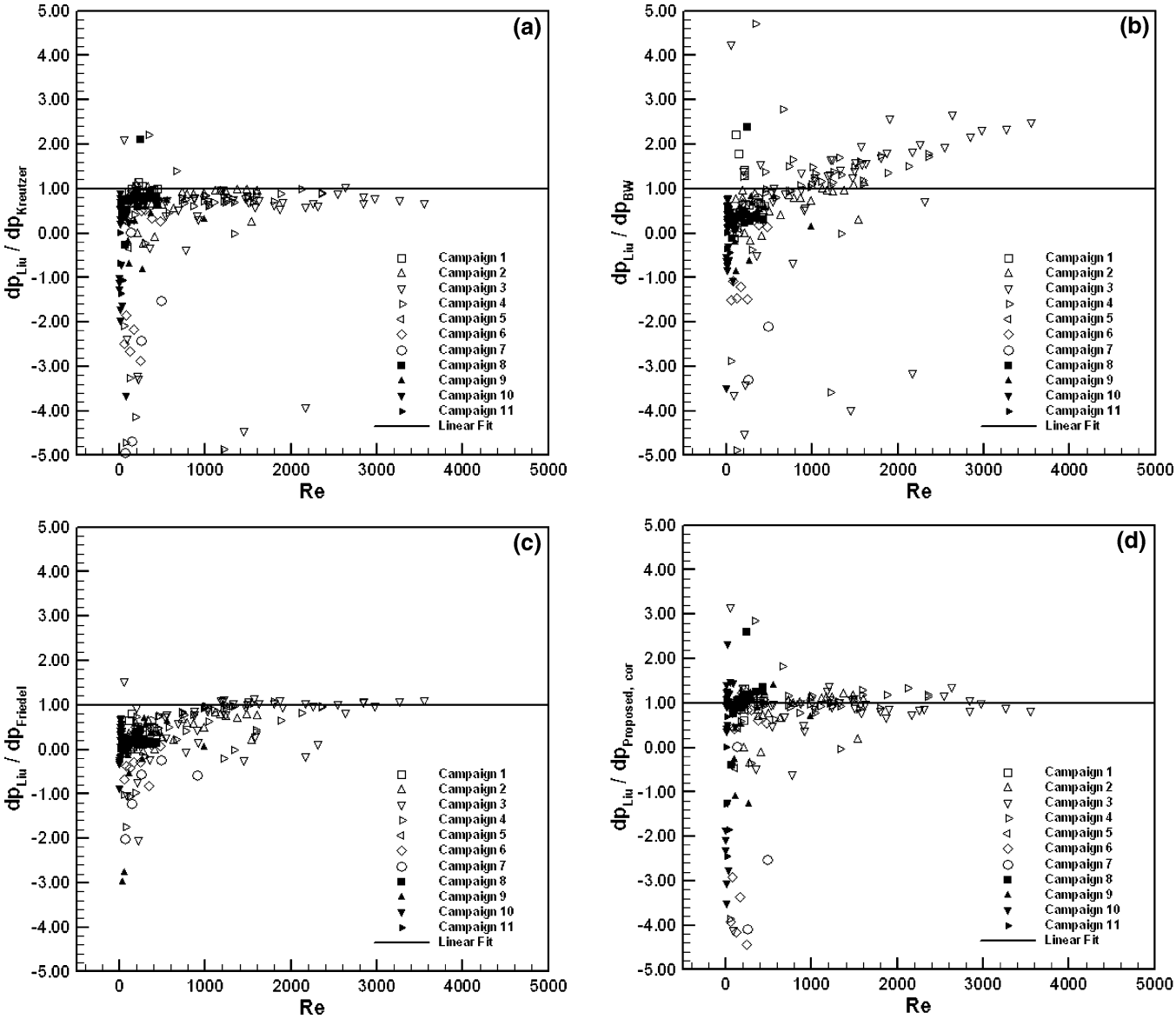

Figure 8. Comparison between the Liu et al.[14] experimental frictional pressure gradients and some empirical correlations for vertically upward flows: (a) correlation of Kreutzer et al.,[13] (b) correlation of Beattie and Whalley,[33] (c) correlation of Friedel,[34] and (d) our correlation.

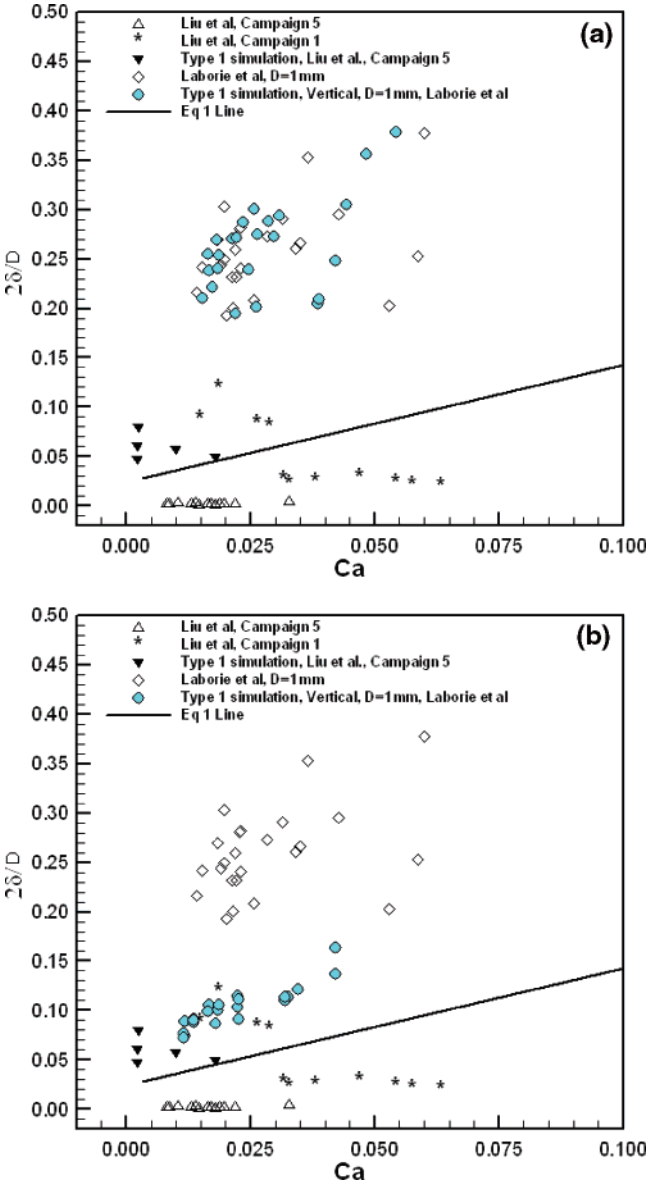

Figure 9. Comparison of film thicknesses estimated from the experimental data and calculated from our type 1 simulations, (a) near the bubble central location and (b) near the bubble front location.

and minichannels and is crucial to the operation of systems that rely on gas−liquid two-phase flow in minichannels. Monolithic catalytic converters represent one of the most important applications of capillaries that operate subject to the Taylor flow regime. Taylor flow regime is morphologically relatively simple and has been extensively simulated in the past using CFD techniques. However, the past CFD models have either assumed a fixed gas−liquid interfacial geometry or have modeled the gas−liquid interphase movement based on the method of spines, which imposes some restrictions on the free movement of the interface.

In this study, the feasibility of CFD modeling of the Taylor flow regime by using the volume-of-fluid (VOF) technique for the motion of the gas−liquid interphase was demonstrated. Using the Fluent[25] CFD code, some experimental data of Laborie et al.[12] for Taylor flow in a 1-mm-diameter capillary and a few data of Liu et al.[14] (Campaign 5) were modeled, with good overall agreement between simulation results and data.

The prediction of the simulation technique agreed with the bubble absolute velocity correlation by Liu et al.[14] Better correlation for slug length prediction in capillaries is proposed based on the experimental data of Liu et al.[14] and Laborie et al.[12] The frictional pressure gradients were also shown to be in fair agreement with the empirical correlations of Kreutzer et al.[13] and Liu et al.[14] A correlation for frictional pressure drop was also proposed. Liquid film thicknesses were estimated from the experimental data of Laborie et al. and Liu et al. and were compared with simulations. The simulation-based film thicknesses representing the vicinity of the bubble front compared reasonably well with the correlation of Aussillous and Quéré[7] (eq 1), within a factor of ∼2.

Notation

a = constant term in eq 3
C_0 = distribution coefficient in drift flux model
Ca = capillary number, $\mu_L U_B/\sigma$
Ca_L = capillary number, $\mu_L U_{TP}/\sigma$
D = diameter (m)
f = Fanning friction factor
g = gravitational constant (m/s^2)
L = capillary length (m)
L_G = Taylor bubble length (m)
L_{slug} = liquid slug length (m)
L_{UC} = unit cell length, $L_G + L_{slug}$ (m)
P = pressure (Pa)
Re = mixture Reynolds number, $\rho_L(U_{LS} + U_{GS})D/\mu_L$
Re_G = gas Reynolds number, $(\rho_G U_{GS} D)/\mu_G$
Re_L = liquid Reynolds number, $(\rho_L U_{LS} D)/\mu_L$
U_B = bubble absolute velocity (m/s)
U_{LS} = superficial liquid velocity (m/s)
U_{GS} = superficial gas velocity (m/s)
U_{TP} = mixture volumetric flux, $U_{GS} + U_{LS}$ (m/s)
V_B = bubble volume (m^3)
V_{gj} = gas drift velocity (m/s)
z = axial coordinate (m)

Greek Symbols

α = gas holdup
β_G = flow volumetric quality, $U_{GS}/(U_{GS} + U_{LS})$
δ = liquid film thickness, (m)
μ = dynamic viscosity (Pa s)
ρ = density (kg/m^3)
σ = surface tension (N/m)

Subscripts

B = bubble
f = friction, fluid
G = gas
H = hydraulic
L = liquid
S = superficial
TP = two-phase

Greek Subscripts

∞ = ambient

Literature Cited

(1) Triplett, K. A.; Ghiaasiaan, S. M.; Abdel-Khalik, S. I.; Sadowski, D. L. Gas−liquid two-phase flow in microchannels. Part I: Two-phase flow patterns. *Int. J. Multiphase Flow* **1999**, *25*, 377−394.

(2) Ghiaasiaan, S. M.; Abdel-Khalik, S. I. Two-phase flow in microchannels. *Adv. Heat Transfer* **2001**, *14*, 145−254.

(3) Heiszwolf, J. J.; Engelvaart, L. B.; Vanden Eijnden, M. G.; Kreutzer, M. T.; Kapteijn, F.; Moulijn, J. A. Hydrodynamic aspects of the monolith loop reactor. *Chem. Eng. Sci.* **2001**, *56*, 805−812.

(4) Nijhuis, T. A.; Kreutzer, M. T.; Romijn, A. C. J.; Kapteijn, F.; Moulijn, J. A., Monolithic catalysts as efficient three-phase reactors. *Chem. Eng. Sci.* **2001**, *56*, 823.

(5) Bretherton, F. B. The motion of long bubbles in tubes. *J. Fluid Mech.* **1961**, *10*, 166−188.

(6) Taylor, G. I. Deposition of a viscous fluid on the wall of a tube. *J. Fluid Mech.* **1961**, *10*, 161−165.

(7) Aussillous, P.; Quéré, D. Quick deposition of a fluid on the wall of a tube. *Phys. Fluids* **2000**, *12*, 2367−2371.

(8) Heil, M. Finite Reynolds number effects in the Bretherton problem. *Phys. Fluids* **2001**, *13*, 2517−2531.

(9) Thulasidas, T. C.; Abraham, M. A.; Cerro, R. L. Bubble-Train Flow in Capillaries of Circular and Square Cross-Section. *Chem. Eng. Sci.* **1995**, *50*, 183−199.

(10) Thulasidas, T. C.; Abraham, M. A.; Cerro, R. L. Flow patterns in liquid slugs during bubble-train flow inside capillaries. *Chem. Eng. Sci.* **1997**, *52*, 2947−2962.

(11) Bercic, G.; Pintar, A. The Role of Gas Bubbles and Liquid Slug Lengths on Mass Transport in the Taylor Flow through Capillaries. *Chem. Eng. Sci.* **1997**, *52*, 3709−3719.

(12) Laborie, S.; Cabassud, C.; Durand-Bourlier, L.; Laine, J. M. Characterisation of Gas−Liquid Two-Phase Flow inside Capillaries. *Chem. Eng. Sci.* **1999**, *54*, 5723.

(13) Kreutzer, M. T.; Kapteijn, F.; Moulijn, J. A.; Kleijn, C. R.; Heiszwolf, J. J. Inertial and interfacial effects on the pressure drop of Taylor flow in capillaries. *AIChE J.* **2005**, *51* (9), 2428−2440.

(14) Liu, H.; Vandu, C. O.; Krishna, R. Hydrodynamics of Taylor flow in vertical capillaries: Flow regimes, bubble rise velocity, liquid slug length, and pressure drop. *Ind. Eng. Chem. Res.* **2005**, *44*, 4884−4897.

(15) Wolffenbuttel, B. M. A.; Nijhuis, T. A.; Stankiewicz, A.; Moulijn, J. A. Novel method for nonintrusive measurement of velocity and slug length in two- and three-phase slug flow in capillaries. *Meas. Sci. Technol.* **2002**, *13*, 1540−1544.

(16) Edvinsson, R.; Irandoust, S. Finite-element analysis of Taylor flow. *AIChE J.* **1996**, *42*, 1815−1823.

(17) Fluid Dynamics International, Inc. 1991.

(18) Kistler, S. F.; Scriven, L. E. Coating flows. In *Computational Analysis of Polymer Processing*; Pearson, J. K. A., Richardson, S. M., Eds.; Applied Science: London, 1984; pp 243−299.

(19) Giavedoni, M. D.; Saita, F. A. The axisymmetric and plane cases of a gas phase steadily displacing a Newtonian liquid−A simultaneous solution of the governing equations. *Phys. Fluids* **1997**, *9*, 2420−2428.

(20) Giavedoni, M. D.; Saita, F. A. The rear meniscus of a long bubble steadily displacing a Newtonian liquid in a capillary tube. *Phys. Fluids* **1999**, *11*, 786−794.

(21) van Baten, J. M.; Krishna, R. CFD Simulations of mass transfer from Taylor Bubbles Rising in Circular Capillaries. *Chem. Eng. Sci.* **2004**, *59*, 2535−2545.

(22) van Baten, J. M.; Krishna, R. CFD Simulations of wall mass transfer for Taylor flow in circular Capillaries. *Chem. Eng. Sci.* **2005**, *60*, 1117−1126.

(23) *ANSYS CFX*, version 4.4; ANSYS Inc.: Canonsburg, PA, 2004.

(24) Taha, T.; Cui, Z. F. CFD modeling of slug flow in vertical tubes. *Chem. Eng. Sci.* **2006**, *61*, 676−687.

(25) *Fluent 6.2.16 User's Guide*; Fluent, Inc.: Lebanon, NH, 2005.

(26) *Gambit 2.2.30 User's Guide*; Fluent, Inc.: Lebanon, NH, 2005.

(27) Laborie, S. Private communcation. E-mail: laborie@lgpm.ecp.fr.

(28) Suo, M.; Griffith, P. Two-phase flow in capillary tubes. *J. Basic Eng.* **1964**, *86*, 576−782.

(29) Mishima, K.; Hibiki, T. Some characteristics of air−water two-phase flow in small diameter vertical tubes. *Int. J. Multiphase Flow* **1996**, *22*, 703−712.

(30) Kariyasaki, A.; Fukano, T.; Ousaka, A.; Kagawa, M. Isothermal air−water two-phase up- and downward flows in a vertical capillary tube (1st report, Flow pattern and void fraction). *Trans. JSME (Ser. B)* **1992**, *58*, 2684−2690.

(31) Nicklin, D. J.; Wilkes, J. O.; Wilkes, J. F. Two-phase flow in tubes. *Trans. Inst. Chem. Eng.* **1962**, *40*, 61−68.

(32) Ghiaasiaan, S. M.; Taylor, K. E.; Kamboj, B. K.; Abdel-Khalik, S. I. Countercurrent two-phase flow regimes and void fraction in vertical and inclined tubes. *Nucl. Sci. Eng.* **1995**, *119*, 182−194.

(33) Beattie, D. R. H.; Whalley, P. B. A simple two-phase frictional pressure drop calculation method. *Int. J. Multiphase Flow* **1982**, *8*, 83−87.

(34) Friedel, L. Improved pressure drop correlations for horizontal and vertical two-phase pipe flow. *3R Int.* **1979**, *18*, 485−492.

Received for review February 6, 2006
Revised manuscript received March 30, 2006
Accepted May 11, 2006

IE0601551